Tunnelling and Underground Space Technology 56 (2016) 79–89

Contents lists available at ScienceDirect

Tunnelling and Underground Space Technology

journal homepage: www.elsevier.com/locate/tust

Velocity and temperature attenuation of a ceiling-jet along a horizontal tunnel with a flat ceiling and natural ventilation

Yasushi Oka [a,*], Hideyuki Oka [b]

[a] Safety Management Course, Faculty of Environment and Information Sciences, Yokohama National University, 79-7 Tokiwadai, Hodogaya-ku, Yokohama 240-8501, Japan
[b] Maritime Risk Assessment Department, National Maritime Research Institute, 6-38-1, Shinkawa, Mitaka, Tokyo 181-0004, Japan

ARTICLE INFO

Article history:
Received 9 July 2015
Received in revised form 17 February 2016
Accepted 3 March 2016
Available online 23 March 2016

Keywords:
Tunnel fire
Ceiling-jet
Velocity attenuation
Temperature attenuation
Stanton number
Richardson number

ABSTRACT

A series of fire tests was conducted in a small-scale tunnel with dimensions of 10.0 m (L) × 0.75 m (W) × 0.45 m (H) and a rectangular cross-section. Detailed measurements of the velocity and temperature within a steady fire-driven ceiling-jet running along the centre of the ceiling were conducted.

Referring to a theoretical derivation process described in the literature as a starting point, correlations representing the velocity and temperature attenuation along the tunnel axis were developed.

The values of the coefficients included in the developed correlation for the velocity attenuation were measured using a particle image velocimetry system during the experiments conducted in the small-scale tunnel. The value of the Stanton number was determined by considering the ceiling-jet thickness, which was derived from the velocity distribution. The values of the coefficients included in the developed correlation for the temperature attenuation were also determined based on experimental results described in the literature, which were obtained in a large-scale tunnel constructed using good heat insulation properties.

Through these correlations developed for the velocity and temperature attenuations along the tunnel axis, the variation in the Richardson number of the ceiling-jet based on the distance from the fire source position along the tunnel axis was examined, and the position where the ceiling-jet changed from a shooting flow to a tranquil flow was determined. The boundary positions between the shooting and tranquil flows were determined using correlations between the velocity and/or temperature attenuation, which were compared with the variation in the Richardson number along the tunnel axis to verify their appropriateness.

1. Introduction

Ceiling-jets influence the response of fire detectors and suppression devices installed below a ceiling, which act as a trigger for occupants to take action during a fire, such extinguishing the fire or evacuating the premises. Studies have therefore been conducted to quantify the flow of a ceiling-jet resulting from the impingement of a fire plume. For example, Alpert (1972) conducted a detailed investigation into the horizontal distribution of the temperature and velocity of a ceiling-jet spread radially under an unconfined ceiling, and proposed useful correlations as a function of the ceiling height and heat release rate. Heskestad (1972) investigated the temperature, velocity, and concentration for the combustion product of a ceiling-jet generated from a fire source, which is characterised by a proportional increase in the heat release rate with the power of time, and proposed a set of theoretical modelling relations for a transient ceiling-jet flow. Heskestad and Delichatsios (1989) proposed dimensionless correlations for the maximum ceiling-jet temperature and velocities during the growth of a fire. The present authors conducted a series of experiments on a ceiling-jet flowing under smooth and unconfined horizontal and inclined ceilings, and proposed a series of empirical formulae representing the temperature and velocity attenuation (Oka and Ando, 2013), the thickness of a ceiling-jet (Oka et al., 2010), the temperature and velocity distribution within a ceiling-jet (Oka and Imazeki, 2014a,b), and the entrainment coefficient of a ceiling-jet (Oka et al., 2014).

However, the properties of a ceiling-jet propagating along the ceiling of a tunnel with specific spatial characteristics (i.e., where the longitudinal length is much longer than a cross-sectional distance such as the height or width) are fundamentally different from those under an unconfined ceiling because the ceiling-jet in a tunnel is influenced by the sidewall and differs depending on

* Corresponding author.
E-mail address: y-oka@ynu.ac.jp (Y. Oka).

http://dx.doi.org/10.1016/j.tust.2016.03.001
0886-7798/

Nomenclature

a, b, c, d	coefficients representing the temperature and velocity attenuation
B	tunnel width (m)
Cp	specific heat (J mol^{-1} K^{-1})
f	friction factor (–)
g	acceleration duo to gravity (m s^{-1})
H	tunnel height (m)
l_b	half-width of tunnel (m), $=B/2$
h_T	ceiling-jet thickness derived from temperature distribution, which is defined as the length from the point where temperature drops to half of ΔT_{max} to tunnel ceiling [m]
h_v	ceiling-jet thickness derived from velocity distribution, which is defined as the length from the point at which the velocity drops to half of V_{max} to tunnel ceiling [m]
Q_c	convective heat release rate (kW)
x	horizontal distance from the centre of the fire source (m)
Pr	Prandtl number (–)
Ri	Richardson number (–)
St	Stanton number (–)
T	temperature (K)
V	velocity
z	vertical distance from tunnel ceiling surface (m)
ΔT	temperature rise (K)
Q_c^*	dimensionless heat release rate (–), $= Q_c/(\rho_\infty C_p T_\infty g^{1/2} H^{5/2})$

Subscripts

max	maximum
∞	atmosphere

the presence or absence of forced ventilation. Most studies on ceiling-jets within a tunnel have focused on the temperature attenuation along the tunnel axis (Hu et al., 2005a,b). Lee and Ryou (2005) carried out reduced-scale experiments to analyse the effects of the aspect ratio on both the smoke temperature attenuation and critical ventilation during a tunnel fire. Li, L. et al. (2011) conducted numerical experiments to develop a simple correlation for the temperature attenuation of a fire-induced flow along the tunnel axis using the changing aspect ratio of a tunnel with a rectangular cross-section and natural ventilation. Hu et al. (2007) conducted two large-scale tunnel fire tests and ten full-scale tests, and presented the temperature attenuation along the tunnel axis with and without longitudinal ventilation. Ingason and Li (2010) represented the dimensionless gas temperature beneath a tunnel ceiling using the sum of two exponential equations based on a comparison of the data from both small- and full-scale tunnel fire tests. Kashef et al. (2013) carried out a series of experimental tests using 1/15 reduced-scale tunnels with a natural ventilation shaft along the tunnel ceiling to investigate the ceiling temperature distribution and smoke diffusion. Li et al. (2012) proposed the correlation to represent the temperature distribution of fire-induced flow along the ceiling of tunnel or corridor with longitudinal ventilation by applying exponential or power function, which changes depending on the distance from fire source, considering the maximum temperature rise and its position. Liu et al. (2016) proposed correlations to predict the maximum smoke temperature rise and the temperature attenuation along the tunnel axis by introducing the sectional coefficient, which is defined as tunnel cross-sectional area divided by the square of height, to describe geometrical characteristic of the tunnel cross- section under longitudinal ventilation. The temperature attenuation along an inclined tunnel ceiling has also been studied, and the empirical correlations, including the tunnel slope, have been proposed (Hu et al., 2013; Hou et al., 2015). However, little research has been conducted on velocity attenuation (Mizutani and Horiuchi, 1988).

Delichatsios (1981) developed correlations for a steady-state ceiling-jet temperature based on the equation of continuity and energy conservation applied to a one-dimensional tranquil flow under a beamed ceiling. The temperature correlation is derived based on the concept that the temperature attenuation of a ceiling-jet is mainly due to friction with the ceiling and heat losses to the ceiling, which in addition to the flow properties, depend on the heating history of the ceiling and the boundary condition (e.g., insulated or constant temperature ceiling). The air entrainment was neglected, and the velocity was calculated using the estimated temperature rise. Koslowski and Motervalli (1994) proposed a recast correlation for the temperature attenuation of a ceiling-jet flow in a primary beamed channel using a non-dimensional temperature rise, instead of the centre line plume conditions at the ceiling. They conducted additional measurements for a range of beam-depth to ceiling-height ratios, where the recast correlation is generalizable. Li, S. et al. (2011) developed correlations for a steady-state ceiling-jet temperature and velocity in both one-dimensional shooting flow and tranquil flow regions, which apply to a corridor. They employed a numerical approach by solving simultaneously the continuity, momentum, and energy conservation equations. Alpert's theory was applied in an axisymmetric radial ceiling-jet region. In a one-dimensional shooting flow region, the air entrainment was considered, whereas the friction with the ceiling and the heat losses were neglected. The similar treatment that Delichatsios employed was applied in a one-dimensional tranquil flow region. We developed correlations for the velocity and temperature attenuation for a steady-state ceiling-jet in both one-dimensional shooting flow and tranquil flow regions. An analytical approach was employed based on the continuity, momentum and energy conservation equations. Delichatsios' method, which is a modified version of Alpert's original technique, was applied to an axisymmetric radial ceiling-jet region, and approaches similar to Li's method were applied to one-dimensional shooting flow and tranquil flow regions.

The current work has two objectives: first, to develop easy-to-use empirical correlations to represent the velocity and temperature attenuation of a ceiling-jet propagating along the tunnel axis in a horizontal tunnel with a smooth and flat ceiling, and second, to estimate the position where a tranquil flow starts based on the variation in the Richardson number based on the distance from the fire source along the tunnel axis.

2. Experimental procedures

A series of fire tests was conducted in a small-scale tunnel with a rectangular cross-section, the dimensions of which are 10.0 m (L) × 0.75 m (W) × 0.45 m (H), as shown in Fig. 1. The tunnel ceiling was built from 12-mm thick calcium silicate board with a smooth surface finish. Both sidewalls were built using a 10-mm thick transparent poly(methyl methacrylate) (PMMA) board. The

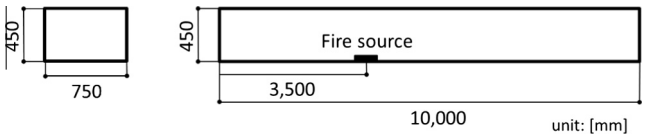

Fig. 1. Small-scale tunnel with rectangular cross-section.

floor was built from 9.5-mm thick plywood, except for the area around the fire source, which was built out of a 12-mm thick calcium silicate board. Both ends of the tunnel were left completely open to allow an unrestricted flow of both the hot gas current flowing out of the tunnel and fresh air being drawn into the tunnel.

The velocities perpendicular to the tunnel ceiling within the ceiling-jet running along the centre of the ceiling were measured using a two-dimensional particle image velocimetry system (2D-PIV). The velocity distributions were obtained at sixteen positions: 0.48, 0.5, 0.52, 0.58, 0.6, 0.62, 0.75, 1.0, 1.5, 2.0, 2.5, 3.0, 3.5, 4.0, 4.4, and 5.5 m from the centre of the fire source. The velocity was measured at least three or four times at each position. A pair of laser sheets pulsed every 0.1 s; the total duration required to acquire 167 pairs of velocity images was 16.7 s. The time interval needed to obtain part of the velocity field image from a pair of velocity image snapshots varied from 1200 to 4500 μs depending on the distance from the fire source. The velocity data were obtained at approximately 4-mm intervals using Koncerto software (Seika Corp.). Oil droplets composed of bis(2-ethylhexyl) sebacate (mean particle size of 1 μm) were used as tracers, and the average discharge velocity at the nozzle was 0.037 m/s.

The temperatures perpendicular to the tunnel ceiling within the ceiling-jet running along the centre of the ceiling were measured using thermocouple rakes consisting of K- and T-type thermocouples with a strand wire diameter of 0.2 mm. Twelve thermocouples were installed in each thermocouple rake. These thermocouple rakes were oriented at 5, 10, 20, 30, 40, 55, 70, 100, 140, 180, 230, and 300 mm from the tunnel ceiling. The temperature distributions were obtained at 13 positions: 0.45, 0.50, 0.55, 0.60, 0.75, 1.0, 1.5, 2.0, 2.5, 3.0, 3.5, 4.4, and 5.5 m from the centre of the fire source. The ceiling gas temperatures resulting from the steady fire source and running along the centre of the ceiling were measured using chromel–alumel (K-type) thermocouples positioned 10-mm below the tunnel ceiling at 40 points spaced every 0.02 m over a distance of −0.1 m to 1.4 m. The strand diameter of the thermocouples was 0.2 mm. The allowable difference of the thermocouple used for the measurements was ±1.5 °C, from −40 °C to 375 °C, and ±0.4% of the measured temperatures were from 375 °C to less than 1000 °C. The measured temperatures included the effect of the heat radiated from the flames and from the heated sides and ceiling of the tunnel.

The concentration of carbon dioxide within the ceiling-jet running along the centre of the ceiling was measured using portable carbon dioxide measuring sensors (GMT221, Viasala; 0–3 vol.%, 0–1 vol.%) set at five positions: 1.5, 2.5, 3.5, 4.5, and 5.5 m from the centre of the fire source. The sensor used for 0–3 vol.% measurements was set at the 1.5-m position from the centre of the fire source and the sensors used for 0–1 vol.% measurements were set at the other positions. These sensors were designed to measure the amount of carbon dioxide in a harsh and humid environment. The length of the gas sensor unit was 60 mm, and each gas sensor was set such that the upper end of the sensor unit was in contact with the ceiling.

Two kinds of fuel, methanol and liquefied petroleum gas (LPG), were employed. A fuel pan of 0.15 m × 0.15 m in size made of 2-mm stainless steel was used to burn the methanol. The fuel mass loss was measured using an electric balance (LP 8200S, Sartorius; readability: 0.01 g), which was set under the small-scale tunnel floor. We provided a small hole for the support strut upon which a fuel pan was placed. The bottom of the fuel pan was positioned at 10 mm above the level of the small-scale tunnel floor.

For the experiment using LPG, the fuel was supplied to a diffusion gas burner of 0.1 m × 0.1 m in size, of which the fine porous aggregate was filled, through a mass flow controller (M100B, MKS Instruments). We set up the square porous burner such that its top surface was at the same level as the small-scale tunnel floor.

The fire sources were positioned at 3.5 m from one end of the tunnel and in the middle of the two sidewalls. The velocity and concentration of carbon dioxide were measured using a 0.15 m × 0.15 m pool fire of methanol, and the temperature was measured using both methanol and LPG.

The heat release rate was estimated from the mass loss or flow rate, and the heat of combustion of the fuel relative to the values was calculated under the assumption of complete combustion. It is generally believed that the source of the driving force of the ceiling-jet is a convective component of the total heat of the combustion. We therefore used the convective heat release rate to analyse the experimental data. We assumed the convective heat resulting from the combustion of the methanol and LPG to be 16.1 and 31.2 MJ/kg, respectively, and the heat of the combustion to be 19.1 and 43.7 MJ/kg, respectively (Tewarson, 2008).

Data on the temperature, mass loss of the fuel, and carbon dioxide concentration were acquired at 1-s intervals using a data logger (MX110, Yokogawa). The data were stored on a PC for further analysis. Data collection started 60 s before the fuel was ignited. Each test ran for at least 10 min. During the tests, forced ventilation in the laboratory was shut down, and all of the doors to the test room were closed.

3. Theoretical approach

Both Delichatsios (1981) and Li, S. et al. (2011) assumed that a density jump takes place after the ceiling-jet intersects the beam or sidewall of the corridor, and that the location where the density jump takes place corresponds to the boundary between Regions II and III. Li, S. et al. (2011) indicated that this location depends upon l_b/H and is within the region of $0.17 < l_b/H < 0.78$. However, this region was originally deduced based on certain assumptions such as a weak fire plume generated from a point source, and sudden changes in the ceiling-jet from a radial flow to an ideal one-dimensional flow. Although the values of l_b/H for both our small-scale tunnel and the reference tunnel are out of the range described above, we assumed that the assumption imposed on the shooting region is conserved within the region up to one or more times the tunnel height, and that the theoretically deduced correlations can be applied.

Following Delichatsios (1981), a ceiling-jet flow was classified into three regions, as shown in Fig. 2. Regions I, II, and III correspond to an axisymmetric radial ceiling-jet region, a one-dimensional shooting flow region, and a one-dimensional tranquil flow region, respectively. Delichatsios (1981) developed a correlation for the temperature attenuation along a beamed ceiling with a focus on Region III by using one-dimensional conservation equations of mass and energy, and excluding the momentum equation. Unlike Delichatsios' model, analytical expressions for the flow properties in Regions II and III were derived from simplified governing equations, including the momentum equation, through the use of a conventional integral method.

As mentioned above, Li, S. et al. (2011) extended Alpert's theory to a one-dimensional ceiling-jet flow. The authors only showed the numerical solutions of their model equations and did not derive the approximate analytical solutions in their work.

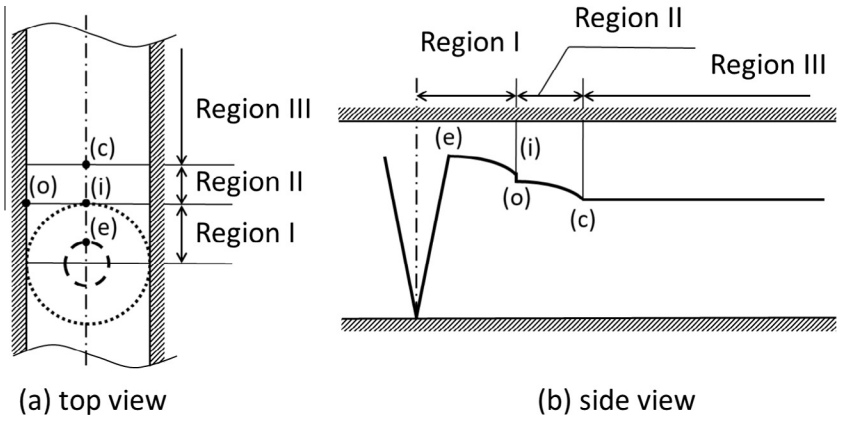

Fig. 2. Schematic diagram of ceiling-jet in horizontal tunnel.

Unlike the theoretical model by Li, S. et al. (2011), instead of Alpert's theory (Alpert, 1975), Delichatsios' approximation technique was applied to the momentum equation (Delichatsios, 1981) in Region I in order to obtain the analytical expressions for the correlations in Regions II and III.

Consequently, the following correlations for Regions II and III can be derived as follows. Eq. (1) is a formula similar to (1-15) and (1-16) and Eq. (2) is a formula similar to (1-25) and (1-26), which are listed in Appendix A.

Region II

$$Y = a\left(\frac{l_b}{H}\right)^{-1/3}\left[1 + b\left(\frac{l_b}{H}\right)^{1/3}\left(\frac{x}{H} - \frac{l_b}{H}\right)\right]^{-1/2}, \quad (1)$$

Region III

$$Y = c\left(\frac{l_b}{H}\right)^{-1/3}\exp\left[d \cdot \mathrm{St} \cdot \left(\frac{l_b}{H}\right)^{1/3}\frac{x}{H}\right], \quad (2)$$

where $Y = (V_{\max}/\sqrt{gH})/Q_c^{*1/3}$, $a = a_v$, $b = b_v$, $c = c_v$, and $d = d_v$ for the velocity and $Y = (\Delta T_{\max}/T_\infty)/Q_c^{*2/3}$, $a = a_T$, $b = b_T$, $c = c_T$, and $d = d_T$ for the temperature. The values of these coefficients and the Stanton number St in Eq. (2) were determined empirically. For further details, the derivation of the above analytical expressions is outlined in Appendix A.

4. Results and discussion

4.1. Heat release rate

The average heat release rate was calculated based data obtained during a quasi-steady state 420–520 s after ignition. The heat release rate was 7.80 ± 0.19 kW. When burning LPG, the heat release rate was adjusted to two different values, 4.48 kW and 8.89 kW.

4.2. Velocity attenuation along the tunnel axis

The velocity distribution perpendicular to the tunnel ceiling was measured at least three or four times at each position, and the mean value was obtained using these multiple data points. Fig. 3 compares the mean velocity distribution at five points from the fire source along the tunnel axis. The velocity distribution at $x/H = 1.07$ showed a maximum velocity at 15 mm below the tunnel ceiling, and exhibited a convex shape with the maximum velocity at the apex. In other words, the velocity decreased exponentially from the apex of the velocity distribution toward the tunnel floor. The velocity distribution at $x/H = 2.22$ showed a different shape at

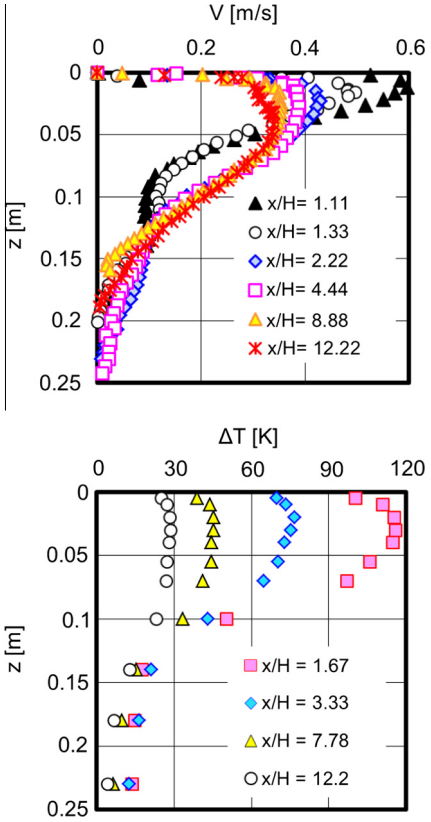

Fig. 3. Typical velocity and temperature distributions within a ceiling-jet at several positions from the fire source.

$x/H = 1.07$; it exhibited a top-hat type distribution with a very slow decrease in velocity from the apex of the velocity distribution toward the tunnel floor. The velocity distribution within a two-dimensional turbulent wall jet, which is a typical flow along a flat plate, was approximated using a top-hat distribution (Verhoff, 1963). Similar velocity distributions of a top-hat type were confirmed within the region of $x/H > 2.22$. The apex of the velocity distribution in this region appeared at around 30 mm below the tunnel ceiling. In addition, the maximum velocity decreased as the distance from the fire source increased with very slow attenuation.

Because the velocity distribution within the ceiling-jet in Region III can be approximated using a top-hat distribution, as shown in Fig. 3, the variation in the ceiling-jet thickness, h_v, can

be derived from the velocity distribution based on the distance from the fire source position along the tunnel axis, as shown in Fig. 4. Instead of directly reading the maximum velocity from the measured velocity distribution, the maximum velocity, V_{max}, was estimated by employing a quadratic fit to three points of the measured data, including the maximum value. The ceiling-jet thickness can be represented through a sum of the momentum boundary layer thickness and the length from the apex to the point at which the velocity drops to half of V_{max} at each position. The thickness of the momentum boundary layer corresponds to the part of the ceiling-jet where the velocity varies from zero to V_{max}. The position at half of V_{max} was estimated by applying a straight-line approximation to three measured points holding the position at half of V_{max}. The value of the ceiling-jet thickness, h_v, was nearly constant in Region III, as shown in Fig. 4. Thus, $h_v/H = 0.226$.

The coefficient d_v in Eq. (2) and the dimensionless ceiling-jet thickness h_v/H have the following relationship: $\frac{h_v}{H} = -\frac{1}{3d_v}\left(\frac{H}{l_b}\right)^{1/3}$. By substituting $h_v/H = 0.226$ and the width and height of the rectangular cross-section of the small-scale tunnel used in the PIV measurement into this correlation, d_V becomes −1.567.

The location of the density jump is known to affect the ceiling-jet behaviour in a tunnel, and can be represented as a function of the tunnel width and height, as shown through $x/H = 0.6(l_b/H)^{-1/3} + (l_b/H)$. The location where the density jump occurs was estimated to be $x/H = 1.471$ using the dimensions of the rectangular cross-section in the small-scale tunnel. In reference to this location, the region before the density jump was assumed to correspond to Region II, and that after the density jump was assumed to correspond to Region III. The values of the coefficients in Eqs. (1) and (2) were determined as the experimental data for each region.

To determine the values of c_v and d_v, an exponential approximation was applied to the experimental results in the region of $1.67 < x/H < 12.2$ (0.75 m < x < 5.5 m), as shown in Fig. 5. The black circles in the figure denote the average values, and the range of maximum and minimum values is denoted using a line segment. The following relations held among proportional constant, the power obtained by applying an exponential approximation, c_v, d_v, l_b/H and the Stanton number.

$$c_v\left(\frac{l_b}{H}\right)^{-1/3} = 0.6176,\quad d_v \cdot \mathrm{St}\left(\frac{l_b}{H}\right)^{1/3} = -0.02231$$

By substituting the dimensions of the rectangular cross-section of the small-scale tunnel, l_b and H, the values of coefficient c_v and the Stanton number were determined to be $c_v = 0.5812$ and St = 0.01513, respectively.

The relationship between St and f can be represented as $\mathrm{St} = \mathrm{Pr}^{-2/3} f/2$. By substituting the values of St = 0.01513 and Pr = 0.7 into this relation, $f = 0.02386$. This value is within the range described by Beyler (1986), where the data of Alpert (1971), Veldman et al. (1975) and You and Faeth (1979) were bound by predictions for $f = 0.02$ and $f = 0.04$.

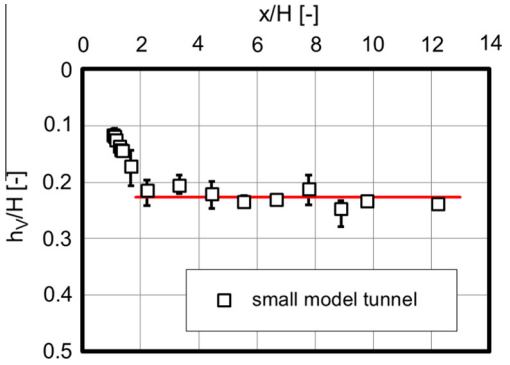

Fig. 4. Ceiling-jet thickness derived from velocity distribution.

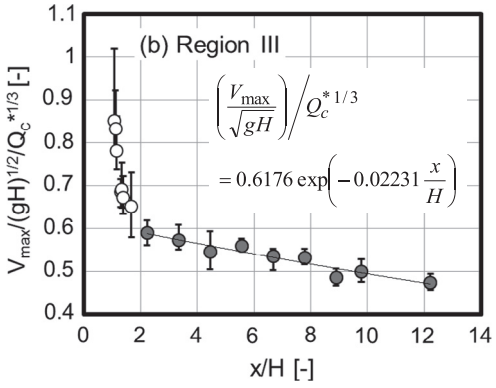

Fig. 5. Velocity attenuation in Region III and approximation formula with exponential function.

The values of the coefficients a_v and b_v were determined as follows. Based on the measured velocity in the region of $1.07 < x/H < 1.38$ ($0.23 < x/H - l_b/H < 0.54$) (i.e., the data in Region II), Eq. (1) was transformed into $\Phi_V = \left\{\left(\frac{V_{max}}{\sqrt{gH}}\Big/ Q_c^{*1/3}\right)/a_v\left(\frac{l_b}{H}\right)^{-1/3}\right\}^{-2} = \left[1 + b_v\left(\frac{l_b}{H}\right)^{1/3}\left(\frac{x}{H} - \frac{l_b}{H}\right)\right]$. The value of a_v was determined to maintain the form of $\Phi_V = \left[1 + b_v\left(\frac{l_b}{H}\right)^{1/3}\left(\frac{x}{H} - \frac{l_b}{H}\right)\right]$, as shown in Fig. 6, which became $a_v = 0.8985$. Based on the value of the slope obtained by applying the linear approximation method, the value of b_v was determined with the aid of the relation $b_v\left(\frac{l_b}{H}\right)^{1/3} = 1.607$. Finally, b_v was determined to be 1.708.

Based on each coefficient determined using the above technique, empirical formulae representing the velocity attenuation along a horizontal tunnel axis with a flat-ceiling and natural ventilation are given in Eq. (3). Here, the Stanton number was St = 0.01513, and the boundary value between Regions II and III was determined as the intersection of the empirical formulae that represent the velocity attenuation in each region.

For Region II ($x/H \leqslant 1.523$),

$$\left(\frac{V_{max}}{\sqrt{gH}}\right)\Big/ Q_c^{*1/3} = 1.126\left(\frac{l_b}{H}\right)^{-1/3}\left[1 + 4.369\left(\frac{l_b}{H}\right)^{1/3}\left(\frac{x}{H} - \frac{l_b}{H}\right)\right]^{-1/2} \quad (3)$$

For Region III ($1.523 < x/H$),

$$\left(\frac{V_{max}}{\sqrt{gH}}\right)/Q_c^{*1/3} = 0.5812\left(\frac{l_b}{H}\right)^{-1/3}\exp\left[-1.567 \cdot \mathrm{St} \cdot \frac{x}{H}\left(\frac{l_b}{H}\right)^{1/3}\right]$$

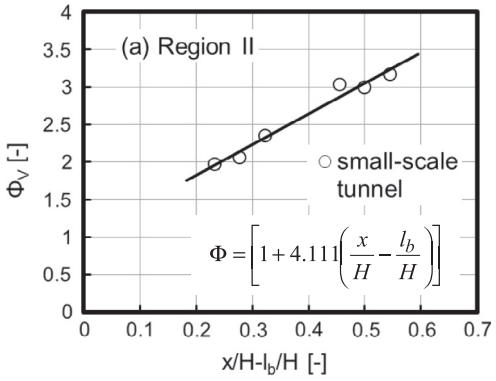

Fig. 6. Method used to determine coefficients a_v and b_v in Region II.

To verify the applicability of the developed empirical formulae to the velocity attenuation, Eq. (3) was compared with experimental results obtained by the Public Works Research Institute of Japan using a full-scale road tunnel having dimensions of 9.8 m (W) × 4.7 m (H) × 400 m (L) and a rectangular cross-section (Mizutani and Horiuchi, 1988). The full-scale road tunnel and experimental conditions are briefly outlined in Appendix B. This full-scale road tunnel was built with reinforced concrete, and upper and lower ducts were installed above and below the roadway with a cross-sectional area of 45.5 m^2. The experiments were conducted on a roadway as the heat release rate was changed in three steps to 1.625, 3.25, and 6.5 MW using methanol. The velocities were measured at a 4.5-m height using a gill-type anemometer 40, 140, and 260 m from the fire source. The velocity data under natural ventilation were read from the literature (Mizutani and Horiuchi, 1988). The empirical formula developed for the velocity attenuation in Region III was confirmed to be able to predict the velocity attenuation in a full-scale road tunnel, as shown in Fig. 7. Such consistency can be explained through the following two ways. First, there was no extreme difference in the rectangular cross-sectional shape between the small-scale tunnel and full-scale tunnel. Second, the ceiling-jet propagated underneath the smooth surface of the flat-ceiling tunnel. We were unable to find the velocity data for Region II. Therefore, verification through a comparison between correlation of velocity attenuation and the experimental data for Region II remains as a future task.

4.3. Temperature attenuation along the tunnel axis

Firstly, we examined the effect of heat radiation using Kaskan's correction method ($T = T_w + \varepsilon\sigma T_w^4 d/(2\lambda)$, Kaskan, 1957), which assumes that the correction value can be obtained from the heat transfer characteristic around an extremely small sphere region remaining within the hot current. The estimated correction value varies depending on the recorded value of each thermocouple and is within the range of 0.65–3.6% under the following condition. The measured temperature rise from the fire source axis to one end of the tunnel along the tunnel axis decreased from 350 to 20 K for a methanol pool fire with an area of 0.15 m × 0.15 m. The emissivity of chromel–alumel alloy is 0.8, and the diameter of the joint region is 0.3 mm, assuming 1.5-times the strand diameter of the thermocouple. It should be noted that the arrangement of the temperature data was conducted based on the recorded value of each thermocouple, namely, that no temperature correction owing to the heat radiation from the thermocouple tip was carried out.

The maximum temperature rise was estimated using a method similar to that applied to the velocity distribution. Fig. 8 compares the temperature attenuation along the tunnel axis for the three kinds of model tunnels: small- and large-scale tunnels and a full-scale road tunnel. Note that the measured temperature positions and measured regions differed for each tunnel experiment. That is, the temperatures in Regions I through III were measured during the small-scale tunnel experiment. The temperatures in Regions II and III were measured during the large-scale tunnel experiment, and those in Region III were measured during the full-scale road tunnel experiment. The temperature of the ceiling-jet within the region of $0.8 < x/H < 3$ in the small-scale tunnel nearly corresponded to that within the large-scale tunnel. However, the temperature within the region of $x/H > 3$ showed a different attenuation along the tunnel axis during each experiment.

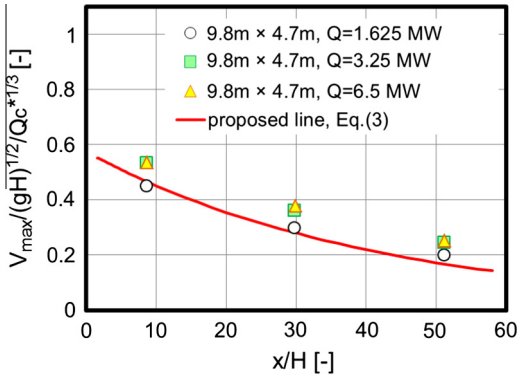

Fig. 7. Applicability of proposed correlation to velocity attenuation.

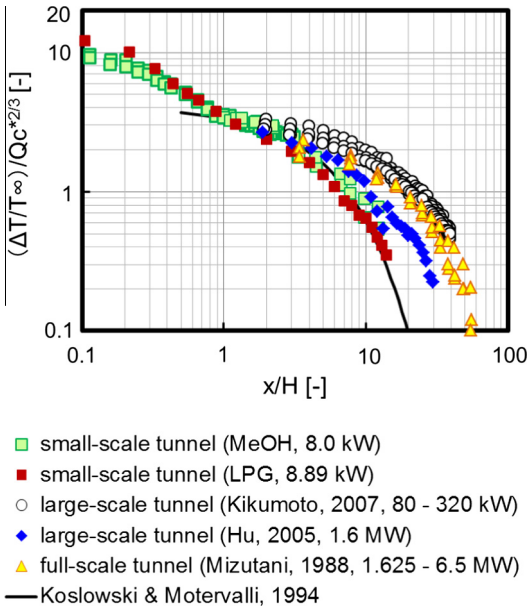

Fig. 8. Comparison of temperature attenuation along the tunnel axis.

The temperature attenuation of Koslowski and Motevalli's correlation shows a similar tendency with that obtained in the small-scale tunnel. In drawing the line obtained by Koslowski and Motevalli's correlation, the tunnel half-width, l_b, and tunnel height, H, were both assigned the dimensions of the small-scale tunnel, and the Stanton number was 0.03, as recommended by Delichatsios. However, the temperature attenuation along the tunnel axis as reported by Hu et al. showed a slower attenuation than that of our small-scale tunnel experiments. However, it attenuated more rapidly than those obtained in both Kikumoto's large-scale tunnel experiment and Mizutani's full-scale tunnel experiment.

This difference can be explained as follows. Fig. 9 shows the variation over time of the measured concentration of carbon dioxide within the steady fire-driven ceiling-jet produced from a fuel pan with dimensions of 0.15 m × 0.15 m during the small-scale tunnel experiment. The maximum velocity in Region III appeared at around 30 mm below the ceiling, as shown in Fig. 3. Based on this position and the physical size of the sensor unit, the reported carbon dioxide concentration corresponded to the representative concentration around the position where the maximum velocity appeared.

Although the concentration of carbon dioxide gradually decreased as the distance from the fire source increased, such concentration within the region of $x/H > 5.56$ showed a nearly constant value because the carbon dioxide never escaped from the ceiling or sidewall. This tendency is quite different from that of the temperature attenuation. The heat escaped through the ceiling and sidewall depending on the thermal insulation properties of the structures, as shown in Fig. 8. Based on the behaviour of the carbon

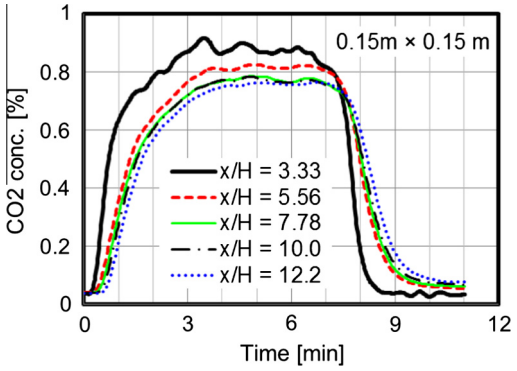

Fig. 9. Variation in carbon dioxide concentration over time within the ceiling-jet generated from a 0.15 m × 0.15 m pool fire using methanol as the fuel.

dioxide concentration, the entrainment of the surrounding air into the ceiling-jet in Region III was quite low, and the temperature attenuation of the ceiling-jet was strongly influenced by the presence or absence of an adjoining duct, the thickness of the material constituting the tunnel, and the thermal insulation properties of the tunnel material.

Therefore, the experimental results obtained in the large-scale tunnel, which had good thermal insulation, were used to determine the coefficients for the temperature attenuation formulae. Appendix C briefly outlines the large-scale tunnel and the experimental conditions applied. The temperature attenuation in Region III was much slower than that of the other tunnels because the thermal insulation was better.

A method similar to that used to calculate a_v and b_v in the velocity attenuation formulae was employed. Eq. (1) in region II was transformed into $\Phi_T = \left\{ \left(\frac{\Delta T_{max}}{T_\infty} \Big/ Q_c^{*2/3} \right) / a_T \left(\frac{l_b}{H} \right)^{-1/3} \right\}^{-2} = \left[1 + b_T \left(\frac{l_b}{H} \right)^{1/3} \left(\frac{x}{H} - \frac{l_b}{H} \right) \right]$, and the value of a_T was determined to maintain the form $\Phi_T = \left[1 + b_T \left(\frac{l_b}{H} \right)^{1/3} \left(\frac{x}{H} - \frac{l_b}{H} \right) \right]$, as shown in Fig. 10. The data from the region of $1.07 < x/H < 1.38$, obtained from the small-scale tunnel experiments, were used. These data were employed because the results from both the small- and large-scale tunnels were very consistent with each other. There were many measurement points along the small-scale tunnel, which was convenient for increasing the reliability in determining the value of the coefficient. The value of a_T became 3.462, and based on the value of the slope obtained by applying the linear approximation method, and with the aid of the relation $b_T \left(\frac{l_b}{H} \right)^{1/3} = 0.6367$,

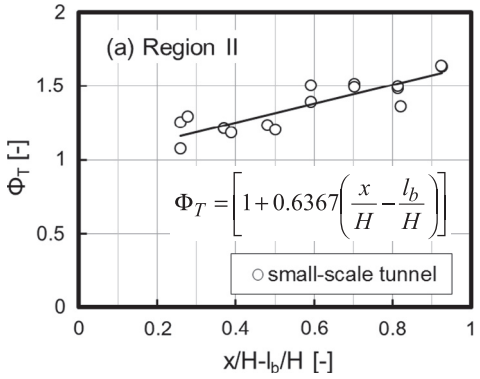

Fig. 10. Method used to determine coefficients a_T and b_T in Region II.

b_T was finally determined to be 0.6765. Here, the value of $l_b/H = 0.833$ was employed for the small-scale tunnel.

Fig. 11 shows a comparison of the temperature attenuation behaviours among the experimental data obtained in a large-scale tunnel by Kikumoto et al. (2007), and two correlations developed by Hu et al. (2005) and Koslowski and Motervalli (1994). In drawing the line obtained by Koslowski and Motevalli's correlation, the tunnel half-width, l_b, and tunnel height, H, were both assigned the dimensions of the large-scale tunnel used in Kikumoto's experiment, where a Stanton number of 0.04, which was the value recommend by Koslowski et al., rather than 0.03, was applied. The correlation for the temperature attenuation derived by Hu et al. (2005) was represented through $\Delta T/\Delta T_0 = 0.95 \exp(-2.72(x - x_0)/L) = 0.95 \exp(-0.037(x - x_0))$, where x is the distance from the fire source, x_0 is defined as 5 m, which corresponds to the first point from the fire source to measure the temperature of smoke layer, and L is set as 74 m, which corresponds to the entire measurement length. This correlation is only available within a region of greater than $x/H > 1.89$. It is clearly confirmed that the temperatures obtained in a large-scale tunnel attenuate much slowly than the other correlations.

To represent the temperature attenuation in Region III, an exponential approximation was therefore applied to the data obtained through the large-scale tunnel experiments for the region $1.91 < x/H < 39.15$, as shown in Fig. 11. The following relations held among the proportional constant, power obtained by applying the exponential approximation, c_T, d_T, l_b/H, and Stanton number. The Stanton number was set to 0.01513, which was the same value employed to develop the velocity attenuation formulae.

$$c_T \left(\frac{l_b}{H} \right)^{-1/3} = 3.113, \quad d_T \cdot \mathrm{St} \left(\frac{l_b}{H} \right)^{1/3} = -0.04811$$

By substituting the dimensions of the rectangular cross-section of the large-scale tunnel, $l_b/H = 0.9630$. The values of the coefficients c_T and d_T became 3.074 and −3.220, respectively.

Based on each coefficient determined using the method described above, the empirical formulae represent the temperature attenuation along a horizontal tunnel axis with a flat ceiling and natural ventilation can be given through Eq. (4). Note that the val-

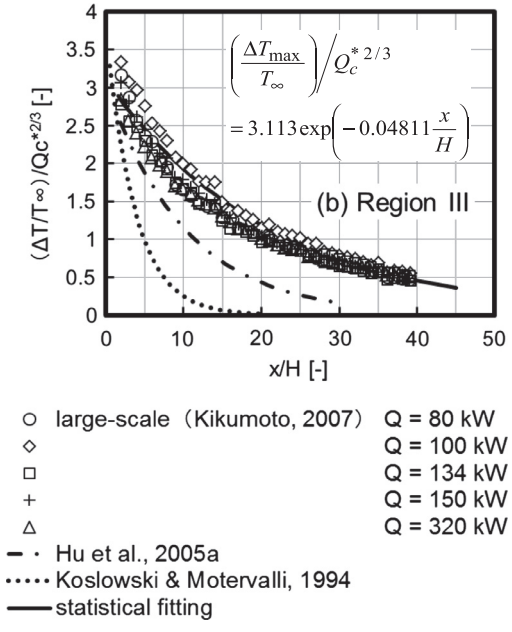

Fig. 11. Temperature attenuation in Region III and application of exponential approximation.

ues of l_b/H differ in Regions II and III because the experimental data came from tunnels with different aspect ratios for the rectangular cross-section.

For Region II ($x/H \leqslant 1.896$),

$$\left(\frac{\Delta T_{max}}{T_\infty}\right)\Big/ Q_c^{*2/3} = 3.462\left(\frac{l_b}{H}\right)^{-1/3}\left[1 + 0.6765\left(\frac{l_b}{H}\right)^{1/3}\left(\frac{x}{H} - \frac{l_b}{H}\right)\right]^{-1/2} \quad (4)$$

For Region III ($1.896 < x/H$),

$$\left(\frac{\Delta T_{max}}{T_\infty}\right)\Big/ Q_c^{*2/3} = 3.074\left(\frac{l_b}{H}\right)^{-1/3}\exp\left[-3.220 \cdot \mathrm{St} \cdot \frac{x}{H}\left(\frac{l_b}{H}\right)^{1/3}\right]$$

Based on the determined value of d_T, the viability of Eq. (4) was verified by comparing the thermal thickness of the ceiling-jet obtained during the small-scale tunnel experiment.

The coefficient d_T in Eq. (4) and the dimensionless thermal thickness h_T/H of the ceiling-jet hold the following relationship: $\frac{h_T}{H} = -\frac{2}{3d_T}\left(\frac{H}{l_b}\right)^{1/3}$. By substituting the dimensions of the rectangular cross-section of the small-scale tunnel, h_T/H became 0.2200. The thermal thickness obtained during the experiments was $h_T/H = 0.2639$. Although the thermal thickness of the ceiling-jet calculated based on the value of d_T was slightly less than the measured value, Eq. (4) was determined to be sufficiently applicable as an engineering tool.

4.4. Variation of Richardson number along the tunnel axis

Fig. 12 shows the variation in the Richardson number of the ceiling-jet with the distance from the fire source. The Richardson number was defined as $\mathrm{Ri} = \frac{\Delta T_{max}}{T_\infty}\frac{g \cdot L_V}{V_{max}^2}$, which is similar to the formula used by Delichatsios (1981). The temperature rise and velocity at an arbitrary position were calculated using Eqs. (3) and (4). The ceiling-jet thickness h_v was also determined using the measured data shown in Fig. 4, and the developed correlation was used for the calculation. The Richardson number in Region II increased linearly with distance from the fire source, whereas that in Region III showed an almost constant value in the region $x/H \geqslant 1.625$. Although the Richardson number should ideally be at unity in Region III, the calculated results from Eqs. (3) and (4), along with h_v, indicated that $\mathrm{Ri} \approx 1.80$.

The variation in the Richardson number at around $x/H = 1.6$ is thought to have been caused by the difference in the boundary points between Regions II and III, which were determined for each correlation based on the temperature, velocity, and thickness.

The boundary location for the temperature attenuation between Regions II and III was $x/H = 1.896$, whereas that for velocity attenuation was $x/H = 1.523$. These locations were defined as the intersection of two lines in each region. The location where the Richardson number became almost constant was therefore close to the boundary location obtained through Eqs. (3) and (4), which indicates that a density jump changes the ceiling-jet properties.

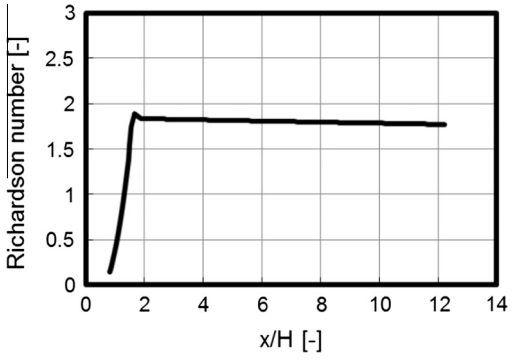

Fig. 12. Variation in Richardson number with distance from the fire source.

5. Conclusions

From a series of experiments focusing on a ceiling-jet running along a horizontal tunnel with a rectangular cross-section, the following conclusions were derived.

(1) New correlations to estimate the attenuation in ceiling-jet velocity and temperature rise along a horizontal tunnel axis were developed using methods employed by Delichatsios and Li et al. The ceiling wall friction and heat transfer were assumed to be negligible in the shooting flow region (Region II), and only air entrainment was considered in the tranquil flow region (Region III). The coefficients were determined through a comparison with the experimental results obtained. When applying the newly developed correlations to different tunnels having extremely different cross-sectional shapes (e.g., a tunnel with a greater height than width), it is necessary to note that the values of the coefficients in the developed correlations may change.

(2) The thermal and momentum thicknesses of the ceiling-jet calculated using the developed coefficients d_v and d_T corresponded closely to the measured results.

(3) Based on the variation in the Richardson number of the ceiling-jet with the distance from the fire source, the location where the ceiling-jet changed from a shooting flow to tranquil flow was about $x/H = 1.610$ in the employed small-scale tunnel.

Acknowledgements

Part of this work was conducted with the support of Grants-in-Aid for Scientific Research (Basic Research B, No. 23310108). This research was conducted with the support of the Joint Usage/Joint Research Centre of the "Research Center for Fire Safety Sciences", which is made up of the Center for Fire Science and Technology, Tokyo University of Science. The authors thank Prof. Matsuyama of Tokyo University of Science for carrying out the particle image velocimetry measurements. The authors thank Mr. Kosuke Nozawa and Mr. Ken Fujii, graduate students of Yokohama National University, for their help with carrying out the experiments.

Appendix A. Derivation of analytical solutions in Regions II and III

The derivation of approximate analytical solutions for a one-dimensional ceiling-jet flow is briefly described below. The governing equations are the same as those of the simple model developed by Li, S. et al. (2011):

Continuity equation: $\frac{d}{dx}\int_0^\infty \rho v B dz = \rho_\infty E V B$,
Momentum equation: $\frac{d}{dx}\int_0^\infty \rho v^2 B dz = -\tau_w B - \frac{d}{dx}\int_0^\infty (\rho_\infty - \rho) g z B dz$,
Energy equation: $\frac{d}{dx}\int_0^\infty \rho v C_p (T - T_\infty) B dz = -q'' B$,
State equation: $\rho T = \rho_\infty T_\infty = \text{constant}$.

To simplify the governing equations, the conventional integral method (Ellison and Turner, 1959) was used as follows:

$$Vh = \int_0^\infty v dy,$$
$$V^2 h = \int_0^\infty v^2 dy,$$
$$Vh\nabla = \int_0^\infty vg\frac{(\rho-\rho_\infty)}{\rho_\infty} dy,$$
$$Sh^2\nabla = \int_0^\infty g\frac{(\rho-\rho_\infty)}{\rho_\infty} y dy,$$

where V is the characteristic velocity, h is the ceiling-jet thickness, ∇ is the characteristic density defect, and S is a shape parameter. Substituting these average properties and introducing Reynolds' analogy between the heat transfer and fluid friction, the conservative equations can be transformed into the following set of equations in dimensionless form (Alpert, 1971):

$$\frac{d\bar{h}}{d\bar{x}} = \frac{(2-S\mathrm{Ri})E - S\cdot\mathrm{Ri}\cdot\mathrm{St} + \bar{f}/2}{1-2S\cdot\mathrm{Ri}}, \tag{1-1}$$
$$\frac{d\mathrm{Ri}}{d\bar{x}} = \frac{\bar{f}/2 + (1+S\cdot\mathrm{Ri})(-1/3\mathrm{St}+E)}{(\bar{h}/3\mathrm{Ri})(1-2S\cdot\mathrm{Ri})}, \tag{1-2}$$
$$\frac{\bar{V}}{\bar{V}_0} = \left(\frac{\mathrm{Ri}_o}{\mathrm{Ri}}\right)^{1/3}\exp\left[-\frac{1}{3}\mathrm{Pr}^{-2/3}\int_{\bar{x}_0}^{\bar{x}}\frac{\bar{f}}{2\bar{h}}d\bar{x}\right], \tag{1-3}$$
$$\frac{\bar{\nabla}}{\bar{\nabla}_0} = \frac{\bar{h}_o}{\bar{h}}\left(\frac{\mathrm{Ri}_o}{\mathrm{Ri}}\right)^{-1/3}\exp\left[-\frac{2}{3}\mathrm{Pr}^{-2/3}\int_{\bar{x}_0}^{\bar{x}}\frac{\bar{f}}{2\bar{h}}d\bar{x}\right], \tag{1-4}$$

where the variables with an over-bar represent non-dimensional quantities, the subscript o denotes the quantities at the initial position in Region II, and St and Pr are the Stanton number and Prandtl number, respectively. These non-dimensional variables are given below:

$$\bar{h} = \frac{h}{H},\ \bar{x} = \frac{x}{H},\ \bar{f} = \frac{\tau_w}{\rho_\infty V^2/2},\ \mathrm{Ri} = \frac{h\nabla}{V^2},$$
$$\bar{V} = \frac{V}{(Q_c g/\rho_\infty C_p T_\infty)^{1/3}H^{-1/3}},\ \bar{\nabla} = \frac{\nabla}{(Q_c g/\rho_\infty C_p T_\infty)^{2/3}H^{-5/3}},$$

where τ_w is the wall shear stress and $\bar{f}$ is the friction factor. Similar to Li., S. et al. (2011), the ceiling temperature was assumed to be equal to the ambient temperature.

Analytical expressions for the correlations of the ceiling-jet thickness with the mean temperature and velocity in Region II are derived here. Compared to Region III, Region II covers a considerably smaller range, so it therefore reasonable to assume that the shear stress and heat transfer on the ceiling are negligible. It is also assumed that the entrainment coefficient E is constant and that the shape factor S is equal to zero. Consequently, the following algebraic equations can easily be obtained from Eqs. (1-1)–(1-4):

$$\bar{h} = 2E(\bar{x}-\bar{x}_o) + \bar{h}_o, \tag{1-5}$$
$$\mathrm{Ri} = \frac{\pi}{2}\cdot\frac{\mathrm{Ri}_e\bar{r}_e}{(\bar{h}_e\bar{r}_e)^{3/2}}\cdot\left(\frac{l_b}{H}\right)^{1/2}\cdot\bar{h}^{3/2}, \tag{1-6}$$
$$\frac{\bar{V}}{\bar{V}_0} = \left(\frac{\mathrm{Ri}_o}{\mathrm{Ri}}\right)^{1/3}, \tag{1-7}$$
$$\frac{\bar{\nabla}}{\bar{\nabla}_0} = \frac{\bar{h}_o}{\bar{h}}\left(\frac{\mathrm{Ri}_o}{\mathrm{Ri}}\right)^{-1/3}. \tag{1-8}$$

Here, the quantities with a subscript o are expressed by those with the subscript e. Unlike the theoretical model by Li, S. et al. (2011), Delichatsios' approximation to the momentum equation (Delichatsios, 1981) is used in Region I instead of Alpert's theory (Alpert, 1975). Delichatsios' approximate equation is written as follows:

$$\frac{q}{(r/r_e)^{1/3}}\cdot\frac{2F^2+1}{2F^{4/3}} \approx \frac{2F_e^2+1}{2F_e^{4/3}}, q = \frac{Vhr}{V_e h_e r_e}, \tag{1-9}$$

where q is the ratio of the flow rate at a certain radial distance to the flow rate at the turning region limit, and F is the Froude number ($F^2 = V^2/\nabla h$). The use of Eq. (1-9) is equivalent to a case in which the relation $\mathrm{Ri}_e = \mathrm{Ri}_i$ is applied to Alpert's analytical solutions. Here, the subscript i denotes the quantities at the position of the intersection with the sidewalls. According to the transition model from a radial jet to a one-dimensional shooting flow (Kunsch, 1999), Li, S., et al. (2011) employed the following correlations:

$$\frac{\mathrm{Ri}_o}{\mathrm{Ri}_i} = \left(\frac{\pi}{2}\right)^4,\quad \frac{\bar{h}_o}{\bar{h}_i} = \left(\frac{\pi}{2}\right)^2,\quad \frac{\bar{V}_o}{\bar{V}_i} = \frac{2}{\pi},\quad \frac{\bar{\nabla}_o}{\bar{\nabla}_i} = 1.$$

As a result, the quantities at the initial position of Region II can be obtained from the analytical solutions for Region I by using the properties at the turning region limit as follows:

$$\bar{h}_o = \left(\frac{\pi}{2}\right)^2\bar{h}_e\cdot\bar{r}_e^{1/3}\left(\frac{l_b}{H}\right)^{-1/3}, \tag{1-10}$$
$$\mathrm{Ri}_o = \left(\frac{\pi}{2}\right)^4\mathrm{Ri}_e, \tag{1-11}$$
$$\bar{V}_o = \left(\frac{4}{\pi^4\mathrm{Ri}_e}\right)^{1/3}\left(\frac{l_b}{H}\right)^{-1/3}, \tag{1-12}$$
$$\bar{\nabla}_o = \left(\frac{\mathrm{Ri}_e}{4\pi^2\bar{r}_e\cdot\bar{h}_e^3}\right)^{1/3}\left(\frac{l_b}{H}\right)^{-1/3}. \tag{1-13}$$

By substituting these quantities into Eqs. (1-5)–(1-8), the approximate analytical solutions for the characteristic properties of a ceiling-jet in Region II can be obtained as follows:

Ceiling-jet thickness,

$$\frac{h}{H} = a_h\left(\frac{x}{H}-\frac{l_b}{H}\right) + b_h\left(\frac{l_b}{H}\right)^{-1/3},\quad a_h = 2E,\quad b_h = \left(\frac{\pi}{2}\right)^2\bar{h}_e\cdot\bar{r}_e^{1/3}, \tag{1-14}$$

Mean velocity,

$$\frac{V/\sqrt{gH}}{Q_c^{*1/3}} = a_V\left(\frac{l_b}{H}\right)^{-1/3}\left[1+b_V\left(\frac{l_b}{H}\right)^{1/3}\left(\frac{x}{H}-\frac{l_b}{H}\right)\right]^{-1/2}; \text{ and}$$
$$a_V = \left(\frac{4}{\pi^4}\right)^{1/3}\mathrm{Ri}_e^{-1/3},\quad b_V = \frac{8E}{\pi^2\bar{h}_e\cdot\bar{r}_e^{1/3}} \tag{1-15}$$

Mean temperature,

$$\frac{(T-T_\infty)/T_\infty}{Q_c^{*2/3}} = a_T\left(\frac{l_b}{H}\right)^{-1/3}\left[1+b_T\left(\frac{l_b}{H}\right)^{1/3}\left(\frac{x}{H}-\frac{l_b}{H}\right)\right]^{-1/2}.$$
$$a_T = \frac{1}{(2\pi)^{2/3}\bar{h}_e}\left(\frac{\mathrm{Ri}_e}{\bar{r}_e}\right)^{1/3},\quad b_T = b_V = \frac{8E}{\pi^2\bar{h}_e\cdot\bar{r}_e^{1/3}} \tag{1-16}$$

Here, the density defect is converted into a temperature rise as follows:

$$\nabla = g\left(\frac{\Delta T}{T_\infty}\right). \tag{1-17}$$

The analytical expressions for the correlations of the ceiling-jet quantities in Region III are derived below. The tranquil flow in Region III develops after the occurrence of the density jump. The location of the density jump is expressed as

$$\bar{x}_c = \frac{\bar{h}_c - \bar{h}_o}{2E+\bar{\tau}} + \frac{l_b}{H}, \tag{1-18}$$

where the subscript c represents the initial position of Region III, i.e., the density jump location. The Richardson number is approximately equal to unity in Region III, and thus the characteristic thickness $\bar{h}_c$ is determined from Eq. (1-6) as follows:

$$\bar{h}_c = \left(\frac{\pi}{2}\right)^{-2/3} \frac{\bar{h}_e \cdot \bar{r}_e}{(\mathrm{Ri}_e \cdot \bar{r}_e)^{2/3}} \left(\frac{l_b}{H}\right)^{-1/3}. \tag{1-19}$$

Because the shear stress on the ceiling is assumed to be negligible in Region II, Eq. (1-18) can be easily transformed into the following equation using substitutions of Eqs. (1-10), (1-18), and (1-19):

$$\bar{x}_c = \frac{1}{2E}\left[\bar{h}_e \cdot \bar{r}_e^{1/3}\left\{\left(\frac{\pi}{2}\mathrm{Ri}_e\right)^{-2/3} - \frac{\pi^2}{4}\right\}\left(\frac{l_b}{H}\right)^{-1/3}\right] + \frac{l_b}{H}. \tag{1-20}$$

The velocity at the density jump location can also be obtained from Eqs. (1-6), (1-7), (1-11), (1-12), and (1-18) as follows:

$$\bar{V}_c = 2^{-2/3}\left(\frac{l_b}{H}\right)^{-1/3}. \tag{1-21}$$

Similarly, the density defect at the density jump location is derived from Eqs. (1-6), (1-8), (1-10), (1-11), (1-13), and (1-19) as follows:

$$\bar{\nabla}_c = \frac{(\pi \mathrm{Ri}_e \cdot \bar{r}_e)^{2/3}}{4\bar{h}_e \cdot \bar{r}_e}\left(\frac{l_b}{H}\right)^{-1/3}. \tag{1-22}$$

According to Delichatsios (1981), the air entrainment can be assumed to be negligible, and the ceiling-jet thickness is almost constant in Region III. In addition, the shear stress on the ceiling is assumed to be constant. As a result, the correlations of the dimensionless velocity and density defect can be derived from Eqs. (1-3) and (1-4) as follows:

For the dimensionless velocity

$$\frac{\bar{V}}{\bar{V}_c} = \exp\left[-\frac{1}{3}\cdot\frac{\mathrm{St}}{\bar{h}_c}\cdot(\bar{x}-\bar{x}_c)\right], \tag{1-23}$$

For the dimensionless density defect

$$\frac{\bar{\nabla}}{\bar{\nabla}_c} = \exp\left[-\frac{2}{3}\cdot\frac{\mathrm{St}}{\bar{h}_c}\cdot(\bar{x}-\bar{x}_c)\right]. \tag{1-24}$$

By substituting Eqs. (1-19)–(1-22) into Eqs. (1-23) and (1-24), the correlations of the mean velocity and temperature in Region III are obtained as follows:

Mean velocity,

$$\frac{V/\sqrt{gH}}{Q_c^{*1/3}} = 2^{-2/3}\exp\left[\frac{1}{3}\mathrm{St}\left\{a + b\left(\frac{l_b}{H}\right)^{4/3}\right\}\right]\cdot\left(\frac{l_b}{H}\right)^{-1/3} \times \exp\left[-\frac{b}{3}\mathrm{St}\left(\frac{l_b}{H}\right)^{1/3}\frac{x}{H}\right], \tag{1-25}$$

Mean temperature,

$$\frac{(T-T_\infty)/T_\infty}{Q_c^{*2/3}} = 2^{-4/3} b \exp\left[\frac{2}{3}\mathrm{St}\left\{a + b\left(\frac{l_b}{H}\right)^{4/3}\right\}\right] \cdot \left(\frac{l_b}{H}\right)^{-1/3}\exp\left[-\frac{2b}{3}\mathrm{St}\left(\frac{l_b}{H}\right)^{1/3}\frac{x}{H}\right]. \tag{1-26}$$

The coefficients a and b are expressed using the quantities at the turning region limit as follows:

$$a = \frac{1}{2E}\left[1 - \left(\frac{\pi}{2}\right)^{8/3}\cdot \mathrm{Ri}_e^{2/3}\right], \quad b = \left(\frac{\pi}{2}\right)^{2/3}\cdot\frac{(\mathrm{Ri}_e\cdot\bar{r}_e)^{2/3}}{\bar{h}_e\cdot\bar{r}_e}. \tag{1-27}$$

The derived correlations for the ceiling-jet properties in Regions II and III contain the quantities at the exit of the turning region. These values can be estimated based on Alpert's (1975) work as follows:

$$\bar{r}_e = \frac{6}{5}\sqrt{\frac{3}{2}E}\left(1 + \frac{\sqrt{3}}{5}E\right)^{-1}, \quad \bar{h}_e = \frac{\sqrt{3}}{5}E\left(1 + \frac{\sqrt{3}}{5}E\right)^{-1}, \quad \mathrm{Ri}_e = \frac{4}{5\sqrt{3}}\cdot\frac{E}{\beta^2+1}, \tag{1-28}$$

where β is the ratio of the width of the density defect profile to that of the velocity profile within a plume.

Appendix B

A full-scale road tunnel with dimensions of 9.8 m (W) × 4.7 m (H) × 400 m (L) was built from reinforced concrete. Ducts were placed on both the upper and lower sides of the roadway with a cross-sectional area of 45.5 m^2, as shown in Fig. A1. The temperature rise, optical smoke density, velocity, and radiative flux were measured. Experiments were conducted in a section of the roadway with different heat release rates in three steps, i.e., 1.625, 3.25, and 6.5 MW. Methanol was employed as the fuel, and a smoke candle was used to visualise the behaviour of the heat flow. Although the details of the heat release rate are not described in the literature, Kikumoto et al. (2007) described the heat release rate of a 8 m^2 fuel pan to be 6.5 MW. Based on this heat release rate, the heat release rate of another fuel pan was estimated in proportion to the pool area.

The velocities were measured at a height of 4.5 m using a gill-type anemometer at 40, 140, and 260 m from the fire source. The velocity data were measured under natural ventilation. The temperatures of the ceiling-jet were measured 0.2 m below the tunnel ceiling using chromel–alumel (K-type) thermocouples.

Appendix C

The dimensions of the large-scale tunnel were 41.0 m (L) × 1.926 m (W) × 1.0 m (H) without an inclination. This model tunnel was built using autoclaved lightweight aerated concrete (ALC) panels with a thickness of 37 mm, and is a 1/3-scale road tunnel for passenger cars.

The temperatures were measured 20 mm below the centre of the tunnel ceiling at interval of 1 m with chromel–alumel (K-type) thermocouples having a strand diameter of 0.1 mm. The heat release rate was changed over five steps, i.e., 80, 100, 134, 150, and 320 kW.

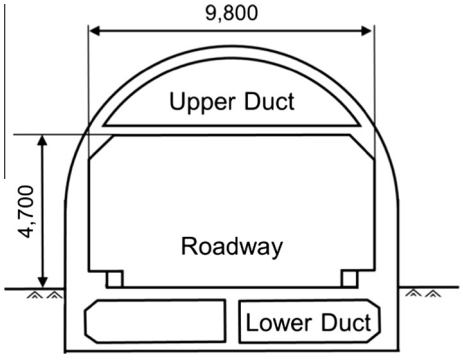

Fig. A1. Outline of full-scale tunnel.

References

Alpert, R.L., 1971. Fire Induced Turbulent Ceiling-jet, Technical Report, FMRC Serial No.19722-2. Factory Mutual Research Corporation.

Alpert, R.L., 1972. Calculation of response time of ceiling-mounted fire detectors. Fire Technol. 8, 181–195.

Alpert, R.L., 1975. Turbulent ceiling-jet induced by large-scale fires. Combust. Sci. Technol. 11, 197–213.

Beyler, C.L., 1986. Fire plume and ceiling-jet. Fire Saf. J. 11, 53–75.

Delichatsios, M.A., 1981. The flow of fire gases under a beamed ceiling. Combust. Flame 43, 1–10.

Ellison, T.H., Turner, J.S., 1959. Turbulent entrainment in stratified flows. J. Fluid Mech. 6, 423–448.

Heskestad, G., 1972. Similarity relations for the initial convective flow generated by fire. American Society of Mechanical Engineers, Paper No.72-WA/HT-17.

Heskestad, G., Delichatsios, M.A., 1989. Update: the initial convective flow in fires. Fire Saf. J. 15, 471.

Hu, L.H., Huo, R., Li, Y.Z., Wang, H.B., Chow, W.K., 2005a. Full-scale burning tests on studying smoke temperature and velocity along a corridor. Tunn. Undergr. Space Technol. 20, 223–229.

Hu, L.H., Huo, R., Wang, H.B., Li, Y.Z., Yang, R.X., He, W.H., 2005b. Full scale experiments on studying smoke spread in a road tunnel, fire safety and science. In: Proceedings of the 8th International Symposium. International Association for Fire Safety Science, pp. 1437–1447.

Hu, L.H., Huo, R., Wang, H.B., Li, Y.Z., Yang, R.X., 2007. Experimental studies on fire-induced buoyant smoke temperature distribution along tunnel ceiling. Build. Environ. 42, 3905–3915.

Hu, L.H., Chen, L.F., Wu, L., Li, Y.Z., Zhand, J.Y., Meng, N., 2013. An experimental investigation and correlation on buoyant gas temperature below ceiling in a slopping tunnel fire. Appl. Therm. Eng. 51, 246–254.

Hou, Y., Gao, Y., Chow, W.K., 2015. A study on ceiling jet characteristics in an inclined tunnel. Tunn. Undergr. Space Technol. 50, 32–46.

Ingason, H., Li, Y.Z., 2010. Model scale tunnel fire tests with longitudinal ventilation. Fire Saf. J. 45, 371–384.

Kashef, A., Yuan, Z., Lei, B., 2013. Ceiling temperature distribution and smoke diffusion in tunnel fires with natural ventilation. Fire Saf. J. 62, 249–255.

Kaskan, W.E., 1957. The dependence of flame temperature on mass burning velocity. In: Proc. 6th (Int.) Symp. on Combust., pp. 134–143.

Kikumoto, T., Kawabata, N., Maruyama, D., Yamada, M., 2007. Model tests on fire smoke behavior in a small road tunnel for passenger cars. J. Jpn. Soc. Civil Engineers, Div. F 63 (3), 361–373 (in Japanese).

Koslowski, C.C., Motervalli, V., 1994. Behavior of a 2-Dimensional Ceiling Jet Flow: A Beamed Ceiling Configuration, Fire Safety and Science, Proceedings of the Fourth International Symposium, International Association for Fire Safety Science, pp. 469–480.

Kunsch, J.P., 1999. Critical velocity and range of a fire-gas plume in a ventilated tunnel. Atmos. Environ. 33, 13–24.

Lee, S.R., Ryou, H.S., 2005. An experimental study of the effect of the aspect ratio on the critical velocity in longitudinal ventilation tunnel fires. J. Fire Sci. 23, 119–138.

Li, S., Zong, R., Zhao, W., Yan, Z., Liao, G., 2011. Theoretical and experimental analysis of ceiling-jet flow in corridor fires. Tunneling Underground Space Technol. 26, 651–658.

Li, L., Cheng, X., Wang, X., Zhang, H., 2011. Temperature distribution of fire-induced flow along tunnels under natural ventilation. J. Fire Sci. 30 (2), 122–137.

Li, L., Li, S., Wang, X., Zhang, H., 2012. Fire-induced flow temperature along tunnels with longitudinal ventilation. Tunneling Underground Space Technol. 32, 44–51.

Liu, F., Yu, L.X., Weng, M.C., Lu, X.L., 2016. Study on longitudinal temperature distribution of fire-induced ceiling flow in tunnels with different sectional coefficients. Tunneling Underground Space Technol. 54, 49–60.

Mizutani, T., Horiuchi, K., 1988. Fire Tests in a Tunnel with Semi-transverse Ventilation System. Public Works Research Institute, Technical Note of PWRI, No.2562 (in Japanese).

Oka, Y., Ando, M., Imazeki, O., 2010. Study on ceiling-jet thickness under an inclined ceiling. Proceedings of 6th International Seminar on Fire and Explosion Hazards, pp. 185–196.

Oka, Y., Ando, M., 2013. Temperature and velocity decreasing property of ceiling-jet impinged on an unconfined inclined ceiling. Fire Saf. J. 55, 97–105.

Oka, Y., Imazeki, O., 2014a. Temperature and velocity distributions of ceiling-jet along an inclined ceiling – part 1: approximation with exponential function –. Fire Saf. J. 65, 41–52.

Oka, Y., Imazeki, O., 2014b. Temperature and velocity distributions of ceiling-jet along an inclined ceiling – part 2: approximation based on cubic function and coordinate transformation. Fire Saf. J. 65, 53–61.

Oka, Y., Yamaguchi, J., Muraoka, K., 2014. Decrease of carbon dioxide concentration and entrainment of horizontally spreading ceiling-jet. Fire Saf. J. 63, 37–42.

Tewarson, A., 2008, Generation of heat and gaseous, liquid, and solid products in fires. In: SFPE Handbook of Fire Protection Engineering, fourth ed., pp. 3–166 (Section 3, Chapter 4).

Veldman, C.C., Kubota, T., Zukoski, E.E., 1975. An experimental investigation of the heat transfer from a buoyant gas plume to a horizontal ceiling, Part 1: Unobstructed ceiling. NBS-GCR-77-97, National Bureau of Standards.

Verhoff, A., 1963. The Two-dimensional Turbulent Wall Jet With and Without an External Stream, Rep.626. Princeton Univ..

You, H.Z., Faeth, G.M., 1979. Ceiling heat transfer during fire plume and fire impingement. Fire Mater. 3, 140–147.